Thermodynamic Analysis on the Fate of Ash Elements in Chemical Looping Combustion of Solid Fuels Iron-Based Oxygen Carriers

N.B. When citing this work, cite the original published paper.

(article starts on next page)

Article

Thermodynamic Analysis on the Fate of Ash Elements in Chemical Looping Combustion of Solid Fuels—Iron-Based Oxygen Carriers

Ivana Staničić,* Joakim Brorsson, Anders Hellman, Tobias Mattisson, and Rainer Backman

Cite This: https://doi.org/10.1021/acs.energyfuels.2c01578

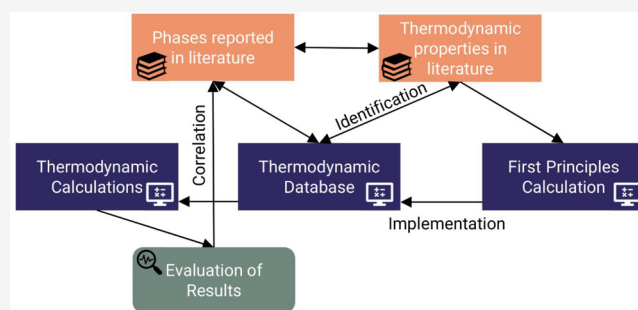Read Online

ACCESS | Metrics & More | Article Recommendations | Supporting Information

ABSTRACT: Chemical looping combustion (CLC) enables efficient combustion of hydrocarbon fuels while also producing a gas stream with high CO_2 concentrations, suitable for carbon capture and storage (CCS). CLC of biomass in combination with CCS results in efficient removal of carbon dioxide from the atmosphere, i.e., negative emissions. However, biomass and waste-derived fuels can contain significant fractions of aggressive ash precursors, which can affect the operability and functionality of oxygen carriers. In this paper, the fate of common ash elements will be investigated thermodynamically in a system utilizing iron-based oxygen carriers: ilmenite and iron oxide. Multiphase, multi-component equilibrium calculations were performed using data-bases from FACT and a user-defined database, with a specific focus on alkali (K and Na) and heavy metals (Cu, Zn, and Pb). A detailed and comprehensive comparison with available literature data from experimental investigations was performed, and compounds not available in the databases were identified. Due to a lack of thermodynamic data in the literature, thermodynamic properties for four compounds, $K_{0.85}Fe_{0.85}Ti_{0.15}O_2$, $K_{0.4}Fe_{0.4}Ti_{0.6}O_2$, KTi_8O_{16}, and $KTi_8O_{16.5}$, were obtained from first-principles calculations. The fate of ash elements is studied for CLC of three biomass and waste-derived solid fuels under relevant CLC conditions: 950 °C in the fuel reactor and 1050 °C in the air reactor. Results show that the choice of the oxygen carriers largely influences the behavior of the ash elements. Compared to CLC with iron oxide, ilmenite is more beneficial with respect to high-temperature corrosion since less potassium is released into the gas phase since the titanium content in ilmenite immobilizes both potassium and calcium. For both oxygen carriers, the most corrosive compounds are expected to leave with the gas in the fuel reactor, keeping the air reactor free from chlorides. It was found that the compound KTi_8O_{16} is stable in reducing conditions and low potassium concentrations. This is in conformity with previous experimental data, where this phase has been identified in the interior of ilmenite particles used in oxygen carrier aided combustion of wood chips.

1. INTRODUCTION

To meet the climate targets agreed upon in the Paris Agreement, greenhouse gas emissions would need to be reduced to zero in less than 20 years. To reach this goal, it is necessary to develop neutral and even negative carbon emission technologies.[1] A considerable amount of CO_2 is generated in the energy sector; therefore, bioenergy with carbon capture and storage (BECCS) is an attractive option since BECCS allows negative emissions while simultaneously producing heat and power.[2] In short, biomass removes CO_2 from the atmosphere through photosynthesis. When biomass is burned or utilized, the carbon returns to the atmosphere. However, if CO_2 is stored, there will be an overall carbon flow out of the atmosphere, i.e., negative emissions. This is necessary if the global average temperature increase should be kept below 2 °C.[1] One technology especially suitable for this purpose is chemical looping combustion (CLC) since both the costs and energy penalty associated with CO_2 capture are among the lowest.[3] Fundamental to the process are metal oxides, referred to as oxygen carriers (OCs), which transport

oxygen between the air reactor (AR) and the fuel reactor (FR), as seen in Figure 1. In the FR, oxygen carriers are reduced by the fuel and are thereafter transported to the AR where the air is used to oxidize the particles before returning to the FR again. In this way, the fuel is converted in a nitrogen-free environment using the oxygen transferred using metal oxides. With this technique, CO_2 is obtained at high concentrations in the FR outlet, which is suitable for carbon capture and storage (CCS).

A transition to the use of renewable energy will likely result in an expansion of the biomass resource base.[4] It is expected that the use of waste fuels will increase; among these are agriculture, municipal solid waste (MSW), and sludge fuels.
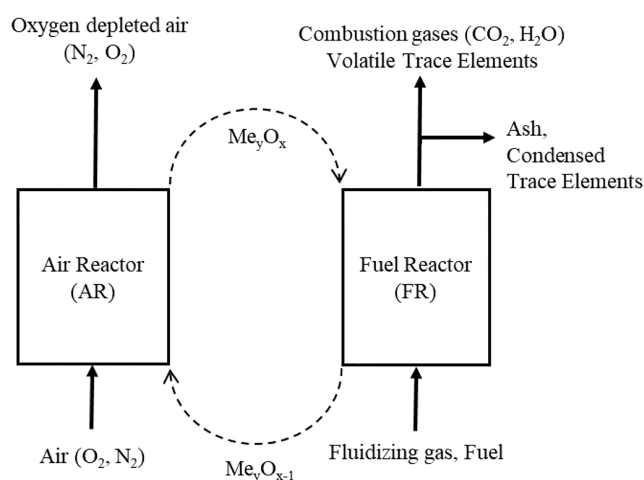
A

Figure 1. Schematic description of chemical looping combustion (CLC).

This implies that clean conversion technologies will be necessary, considering not only carbon but also toxic inorganic elements. Incineration is the conventional way to process this type of fuel, but CLC could have certain advantages. Here, inorganic trace impurities and ash compounds are concentrated in the FR, which is highly advantageous for cleaning and thereby limiting emission and corrosion.[5]

The broadening of biobased fuels also leads to a larger variation in ash amount and composition. Ashes contain inorganic compounds that remain after fuel is combusted. This can be problematic as waste-derived fuels contain elevated concentrations of the alkali metals K and Na and the heavy metals Zn, Cu, and Pb, but also Cl. The alkali and heavy metal chlorides follow the flue gas into the convection path of the boiler where they can cause corrosion and fouling.[6] Since heavy metal chlorides form eutectic mixtures with alkali chlorides, they can induce corrosion at temperatures as low as 250−300 °C.[7] The formation and behavior of these heavy metal compounds are not yet as widely understood as alkali metals, but as the fuel resource base is expanding to include more waste fuels, there has been more focus on heavy metal-induced corrosion.[8] Another problem with complex fuels is that the formation of gaseous alkali chlorides also promotes reaction with silicates due to increased mobility.[9] Alkali silicates, with low melting temperatures, could cause agglomeration and in the worst-case defluidization of a bed.[10] The alkali balance in the boiler is thus affected by the interaction with the bed material.

1.1. Ash Interaction with Iron-Based Oxygen Carriers. Through the years, diverse types of OCs have been studied experimentally and theoretically, both synthetic material and natural ores, with different preparation methods and support materials. As of today, iron-based OCs are among the most abundant, economically viable, and environmentally friendly oxygen carriers.[11] Furthermore, they have high melting temperatures, which reduce the risk of agglomerations.[12] However, a disadvantage is that they show a low oxygen transport capacity compared to other common materials, such as Cu- and Ni-based oxygen carriers.[13] Nevertheless, various iron ores have shown favorable attributes as oxygen carriers and have been used extensively in CLC pilots.[14,15] Mn-based ores have also been shown to be effective OCs due to their chemical looping with oxygen uncoupling (CLOU) property.

A specific focus on Mn-based ores will be given in Part 2 of this study.

The interaction between OCs and ash is important to understand as it could cause deactivation, agglomeration, or attrition of the OC. The outcome depends on ash content, mineralogy, experimental conditions, and OC composition.[16] Agglomerations are, for example, usually caused by a reaction between alkali and silica forming alkali silicates with low melting temperatures.[9,10] Gu et al. found that K- and Si-rich biomass ashes produced molten potassium silicates, causing particle sintering and reactivity deterioration,[17] while K-rich ashes with a low amount of Si improved the reactivity of iron ores in CLC.[17] Ash components at the surface or in the bulk of the OC may alter the reaction kinetics. For example, the reaction rate can be decreased if gas diffusion is hindered by an ash layer formed on the surface of the particles, but ash components on OCs could also have a catalyzing effect on the reaction or even have oxygen carrier properties themselves,[18] for example, $CaSO_4$.[16]

Ilmenite, an iron and titanium ore, has been extensively examined as an OC.[19−22] Ilmenite has good fluidization properties, high melting point, and low production of fines and can be utilized without much pretreatment. Ilmenite has been examined as an oxygen-carrying bed material for oxygen carrier aided combustion (OCAC) at a semi-industrial scale[23] but also in several commercial waste-to-energy (WtE) units in Sweden.[24] When studying ilmenite particles that had been operated in a 12 MW_{th} CFB boiler with biomass as the fuel, it was seen that segregation of Fe to the surfaces and enrichment of Ti in the particle core had taken place.[25−27] A Ca-rich double layer on the particle had also been formed, which surrounded the iron layer.[27] Both the separation of Ti and Fe as well as the Ca layer have been observed previously under chemical looping conditions.[19,28] Other studies have found that, with increased time of exposure, K migrates into the ilmenite particle core[27] and that, depending on the chemical form of K, it will react differently in the matrix.[29] Research conducted on the ash layer build-up and sulfur interaction when using ilmenite in OCAC applications shows that calcium and potassium are bound to sulfur both in and on the ilmenite particles.[27,30] Limited research around the chemistry of heavy metals in chemical looping processes is available. In a series of experiments around OCAC with ilmenite and waste fuels, zinc ferrites were detected between the double calcium layer, and copper ferrites were identified on the particle surface.[31] After increased residence time, copper has been observed in the particle core.[31−33]

Role of Thermodynamic Calculations. Thermodynamic equilibrium calculations have become a widely used tool for predicting ash-related problems during combustion.[34,35] The approach is based on minimizing Gibbs energy which calculates the chemical equilibrium composition of a system considering thermodynamic data of all possible phases and compounds.[35] These calculations do not consider kinetics and transport phenomena, but due to the good gas−solid contact, mixing, and relatively long residence times of solid particles in fluidized beds, the conditions could come close to equilibrium. It is not uncommon to combine experimental tests with thermodynamic predictions.[29,36,37] Most recent studies have used FactSage and associated databases to monitor the slag formation and predict agglomeration behavior in the CLC of coal.[38,39] It was concluded that parameters that affect the bed composition are the ash composition, the ratio of ash to OC,

and the type of OC, which had a significant impact on the rate of agglomeration.[38] It has also been used to predict phase formation in relevant OC—ash systems.

1.2. Aim of Study. This study aims to use multiphase multicomponent thermodynamic equilibrium calculations to monitor phases in the FR and AR while simultaneously studying the effect of different fuels, ash contents in the bed, and the two iron-based oxygen carriers, ilmenite and iron oxide. A few selected elements are in focus and selected based on their role in emission, corrosion, and melt formation: Cl, K, Na, and S along with the important heavy metals Zn, Cu, and Pb previously studied in OCAC.[31,33] The influence of the oxygen carrier on the solid-phase distribution and elements will be discussed along with implications on CLC operation and possible remedies. In this study, we will expand the knowledge regarding the phase formation in CLC to include biomass and waste fuels.

The FactSage 8.1 databases are the main databases employed in this study. To achieve an understanding that is as complete as possible, several tasks were undertaken: (i) a comprehensive and detailed review of available experimental and thermodynamic data on biomass/waste ash and OC interactions, (ii) assessment and incorporation of identified phases in other thermodynamic databases, and (iii) calculation of thermodynamic properties from first-principles for a few selected compounds, for which no thermodynamic data has been reported. This involved combining reaction energies obtained from density functional theory with thermal properties, estimated via the harmonic approximation, using reference data from the NIST-JANAF thermochemical tables.[40] The methodology together with the computational details will be published in a separate paper. This approach allows for the most comprehensive and updated thermodynamic study of these important systems to date.

2. METHOD

2.1. Thermodynamic Software and Databases. Equilibrium calculations are used to determine the stable chemical and physical forms in a system using parameters such as the elemental composition of input streams, temperatures, and pressures. By minimizing Gibbs free energy under a mass balance constraint, one can monitor stable solid and gaseous phases. In this paper, FactSage 8.1 was used along with the databases FactPS, FToxid, and FTsalt and the user-defined database HSCA. The HSCA database comprises data from HSC Chemistry 9 and 10. It has been updated to include heavy metal compounds not available in the FactSage databases. This database has been used in previous work.[31−33]

2.2. First-Principles Calculations. A major limitation for thermodynamic calculations is the availability of experimental equilibrium data. This is apparent in the present study since several experimentally observed crystalline phases could not be found in the commercial FACT databases or in the literature. To circumvent this problem, standard enthalpies of formation and entropies, as well as the temperature variation of the heat capacity, were estimated based on first-principles calculations. The methodology together with the computational details will be published in a separate article. With respect to utilization of first-principles calculations for iron-based oxygen carriers, there have been some previous studies,[41,42,43] although the approach of calculating energetics and heat capacities for inclusion in general multicomponent calculations has not been done previously to our knowledge. The focus has been on a few

key compounds within the K—Fe—Ti—O phase space, namely, $K_{0.4}Fe_{0.4}Ti_{0.6}O_2$, $K_{0.85}Fe_{0.85}Ti_{0.15}O_2$, KTi_8O_{16}, and $KTi_8O_{16.5}$, as well as $FeTiO_3$, which was included as a reference. The reaction energies were computed using density functional theory as well as the phononic contribution to the heat capacity under the harmonic approximation. In accordance with the procedure presented by Benisek and Dachs,[44] the results from these ab initio calculations were combined with experimental data from the NIST-JANAF thermochemical tables to determine the enthalpy and entropy at room temperature together with the temperature dependence of the heat capacity. As a reference, the same approach was applied to ilmenite, which showed a remarkably good agreement with the values in the FACT database. More precisely, the difference was less than 5 J/(mol K) for the entropy as well as the heat capacity, and 2 J/mol in the case of the enthalpy over a wide temperature range (293.15−1200 K). The calculated thermal properties of the compounds $FeTiO_3$, $K_{0.85}Fe_{0.85}Ti_{0.15}O_2$, $K_{0.4}Fe_{0.4}Ti_{0.6}O_2$, KTi_8O_{16}, and $KTi_8O_{16.5}$ are listed in Table S1 in the Supporting Information (SI).

2.3. Modeling Approach. The chemistry and fate of ash elements can be expected to be affected by the composition of the surrounding gas phase. A list of gas-phase compositions recorded in fuel reactor tests published in the literature is summarized in Table S2. The corresponding oxygen partial pressure is recalculated to 950 °C using the CO to CO_2 ratio for the dry gases and full gas composition for the rest. These values are provided to relate and compare with the calculations. A range of different reduction potentials can be expected in the FR, as evident from Table S2, which correlates to the gas conversion. Although measures are being developed to improve gas conversion for solid fuel CLC,[45,46] the use of Fe-based oxygen carriers would likely mean that some unburnt species such as CO and H_2 would be present in the outlet, even at optimized conditions. To compare results with previous experimental findings, the reduction level $\log_{10}(pO_2) = -13.2$ atm is used in the FR for this paper.[37] Two iron-based OCs will be investigated, ilmenite and iron oxide, along with three different fuels: branches and treetops (BT), recycled waste wood (RWW), and municipal solid waste (MSW). Fuels were defined in FactSage according to Table 1. These three fuels have distinctive characteristics concerning the ash content, moisture, and Cl/S concentrations. It is likely that some type of support or more heterogeneous ore would be used as an OC in a real system. Still, to achieve a detailed view of how Fe reacts with ash components, it was decided to utilize pure iron oxide in these calculations.

The amount of oxygen carrier needed to maintain a temperature of 950 °C in the FR was determined with a heat balance over the FR, as it has been shown previously that it is often the transport of sensible heat from the AR to FR that sets the minimum circulation rate required.[47] The following assumptions were made: (i) The FR is adiabatic. (ii) The OC entering the FR is fully oxidized with a temperature of 1050 °C. (iii) The FR is fluidized with CO_2, preheated to 400 °C. Temperature and reduction levels are assumed to be homogeneous in the reactors. The AR is fluidized with air preheated to 400 °C, and the amount is determined individually for each calculation. The oxygen concentration in the AR exhaust gas is 5%.

Accumulation of ash is an important problem in the CLC of solid fuels that requires special attention. Ash typically has a lower density compared to OCs and can be separated by a

Table 1. Fuel Composition of the Three Fuels: Branches and Treetops, Recycled Waste Wood, and Municipal Solid Waste[a]

	unit	branches and treetops (BT)	recycled waste wood (RWW)	municipal solid waste (MSW)
ash	wt % dry	2.6	5.8	13.1
moisture	wt % ar	51.2	23.3	37.1
C	wt % daf	52.5	52.0	58.4
H	wt % daf	6.18	6.31	7.6
O	wt % by diff.	40.5	40.4	30.8
N	wt % daf	0.73	1.17	1.4
S	wt % daf	0.052	0.08	0.76
Cl	wt % daf	0.0031	0.055	1.01
Ash Elements				
Ca	mg/kg ash	192 000	68 000	30 000
Si	mg/kg ash	113 000	116 000	40 000
Al	mg/kg ash	20 000	27 000	13 000
Fe	mg/kg ash	8000	23 000	7000
Ti	mg/kg ash	1000	18 000	2000
Mn	mg/kg ash	16 000	2000	200
Mg	mg/kg ash	21 000	12 000	4000
Na	mg/kg ash	9000	14 000	7000
K	mg/kg ash	76 000	21 000	3000
P	mg/kg ash	17 100	1800	900
Ba	mg/kg ash	2700	3300	300
As	mg/kg ash	3	430	24
Co	mg/kg ash		20	8
Cd	mg/kg ash		8	3.5
Cr	mg/kg ash	110	948	185
Cu	mg/kg ash	110	594	742
Ni	mg/kg ash	40	39	169
Mo	mg/kg ash	4	8	9
Sb	mg/kg ash		13	57
V	mg/kg ash		39	13
Pb	mg/kg ash	74	544	643
Zn	mg/kg ash	2000	10 390	820

[a]Ash composition of the three fuel ashes is presented on an elemental basis.

cyclone. It is also expected during operation that light ash particles can follow the gas phase out from the FR and that the ash is separated from the oxygen carrier before entering the AR. However, some ash may remain in the system, especially when using high-ash-content fuels.[16,48] The transportation of ash could also be due to interaction with the OC or the formation of sticky compounds on the OC surface. Thus, the

fate of ash components in an AR will also be discussed in this paper. In the calculations, all solid phases in the FR will be transferred to the AR to study the worst-case scenario and monitor the phase transitions. This will also show the importance of effective ash separation. The maximum amount of ash investigated is around 65−70 wt % of the total fluidized bed, which is an extreme case that will likely not be achieved with biomass fuels. Waste fuels, on the other hand, contain significantly larger ash fractions. Phase formation with increasing ash concentrations will be presented for each fuel and oxygen carrier to illustrate the effect of ash components. The calculations were performed stepwise starting from the lowest ash amount, according to Table 1, until reaching approximately the same weight as the oxygen carrier. The release of elements will be discussed based on the initial calculation, with the lowest ash concentration. The ash concentration in the bed is calculated as the difference between the total mass of the solid phases and the total reduced OC in the FR (SPINA for iron oxide and ILMEA + TiSP for ilmenite) or oxidized OC in the AR (M_2O_3 for iron oxide and M_2O_3 + TiO_2 for ilmenite) divided by the total mass of the solids and presented in the results as a white dashed line. A summary of the solid solutions and their abbreviations, which are used in this work, are presented in Table S3.

3. RESULTS

Crystalline phases reported for iron-based OCs used in chemical looping applications such as CLC and OCAC ranging from laboratory- to large-scale units are presented in Table 2. Literature data regarding the crystalline phases for chemical looping of biomass and, especially, waste fuels are scarce. There is also limited knowledge on the crystalline phases and behavior of ash elements that cover both the FR and AR. A comparison between phases observed in the literature and those available in FactSage identified several compounds missing in the databases: KTi_8O_{16}, $KTi_8O_{16.5}$, $CaH_2P_2O_7$, $K_{0.85}Fe_{0.85}Ti_{0.15}O_2$, and $K_{0.4}Fe_{0.4}Ti_{0.6}O_2$. A search for thermodynamic data in the literature was performed, but no information regarding energetics was found. Due to a lack of data in the literature, thermodynamic properties for a few specific compounds were estimated based on first-principles calculations. The influence of these compounds on the thermodynamic equilibrium is discussed in Section 3.4.

To evaluate the influence of iron-based OCs on phase formation, each fuel was first studied separately without the oxygen carrier present. The solid-phase distribution in the FR and AR without the oxygen carrier present can be found in Tables S4−S6. These results correlate the phase stability with the specific fuels independent of the oxygen carrier. Below, Sections 3.1−3.3 follow calculations performed using the FACT and HSC databases. The effect of the K−Ti−O and K−Ti−Fe−O phases using energetic data from first-principles calculations will be discussed in Section 3.4.

3.1. Chemical Looping Combustion Using Iron Oxide. From the phase diagram of iron oxide presented in Figure S1, the most reduced form will be Fe_3O_4 (as spinel) in the fuel reactor. Reduction to FeO is preferably avoided due to problems with defluidization and slow oxidation in addition to the fact that full oxidation of fuel will not be possible.[55] The solid-phase distribution in the FR and AR for BT is presented in Figure 2, while results for RWW and MSW can be found in Figures S2 and S3. From Figure 2, with BT-fuel, the main phase is the spinel (Fe_3O_4), and with increasing ash content in

Table 2. Identified Crystalline Phases for Iron-Based Oxygen Carriers Used in Chemical Looping Applications of Biomass and Waste Fuels[a]

oxygen carrier	FR temperature	unit	fuel or model compound	phases identified by XRD	mode	ref
ilmenite	850	tubular furnace	K_2CO_3, K_2SO_4, KCl, KH_2PO_4	$FeTiO_3$, TiO_2, Fe_xO_y, Fe, FeS, K-titanates, KPO_3, P_2O_5	CLC	29
iron mill scale	850	TGA and tubular furnace	K_2CO_3, K_2SO_4, KCl, KH_2PO_4	Fe_2O_3, Fe_3O_4	CLC	49
hematite, ilmenite	900	tubular furnace	$CaCO_3$, K_2CO_3, SiO_2	$Ca_2Fe_2O_5$, $KFeO_2$, K_3FeO_4, $Fe_{2.57}Si_{0.43}O_4$, $K_{0.85}Fe_{0.85}Ti_{0.15}O_2$, $K_{0.4}Fe_{0.4}Ti_{0.6}O_2$, $K_2Ti_2O_5$	CLC	36, 37
ilmenite	900	TGA		$FeTiO_3$, Fe_2O_3, TiO_2, Fe_2TiO_5	CLC	50
ilmenite and silica sand	900	12 MW_{th}	wood chips	$Ca(Fe_{0.3}, Ti_{0.7})O_{2.85}$, KTi_8O_{16}	OCAC	25
ilmenite	850	12 MW_{th}	wood chips	$CaTiO_3$, $KTi_8O_{16.5}$	OCAC	27
iron ore	950	500 W_{th} continuous unit	pine sawdust	Fe_2O_3, SiO_2	CLC	14
hematite	800−900	1 kW_{th} continuous unit	sewage sludge	Fe_3O_4, SiO_2, $CaAl_2Si_2O_8$, $CaH_2P_2O_7$, $CaHPO_4$	CLC	48
iron ore impregnated with $BaAl_2O_4$, $CaAl_2O_4$, and $MgAl_2O_4$	900	fluidized batch reactor	MSW-derived syn-gas	Fe_2O_3, SiO_2, $CaFe_2O_4$, $MgFe_2O_4$	CLC	51
hematite ore, ilmenite ore	1100	calorimetry high-T in situ XRD[b]		$CaFe_2O_4$, $Fe_{2-x}Si_xO_4$, $FeTiO_3$, $CaFe_4O_7$, $(Mg, Fe)_3O_4$, $CaSiTiO_5$	sintering in argon	52
ilmenite and silica sand	880−935	75 MW_{th}	MSW	$(Mg, Zn, Fe)_3O_4$, Fe_2TiO_5, $CaTi_{0.75}Fe_{0.25}O_3$, $(Ca, Na)_2(Mg, Fe, Al)Si_2O_7$, $(K, Na)AlSi_3O_8$, $NaAlSi_2O_6$, $CaSiO_3$, $CaSO_4$	OCAC	33
ilmenite	900	30 kW_{th}	60% bituminous coal and 40% straw	$(K, Na)_2Fe_2O_4$, KTi_8O_{16}, $K_2Ti_6O_{13}$, $KAlSi_3O_8$, $CaSO_4$, $CaAl_2(SiO_4)_2$	OCAC	53
ilmenite and LD-slag	850−900	300 W		$(Fe, Ti)_3O_4$, $(Fe, Ti)_2O_3$, TiO_2	CLC/CLG	54
Australian iron ore	900	fluidized batch reactor	corn stalk, rape stalk, wheat straw	Fe_2O_3, Fe_3O_4, K_3FeO_2, Fe_2SiO_4	CLC	17

[a]Compounds that are not available in thermodynamic databases are presented in italics. [b]Aim not specifically OCAC or CLC but relevant to this study.
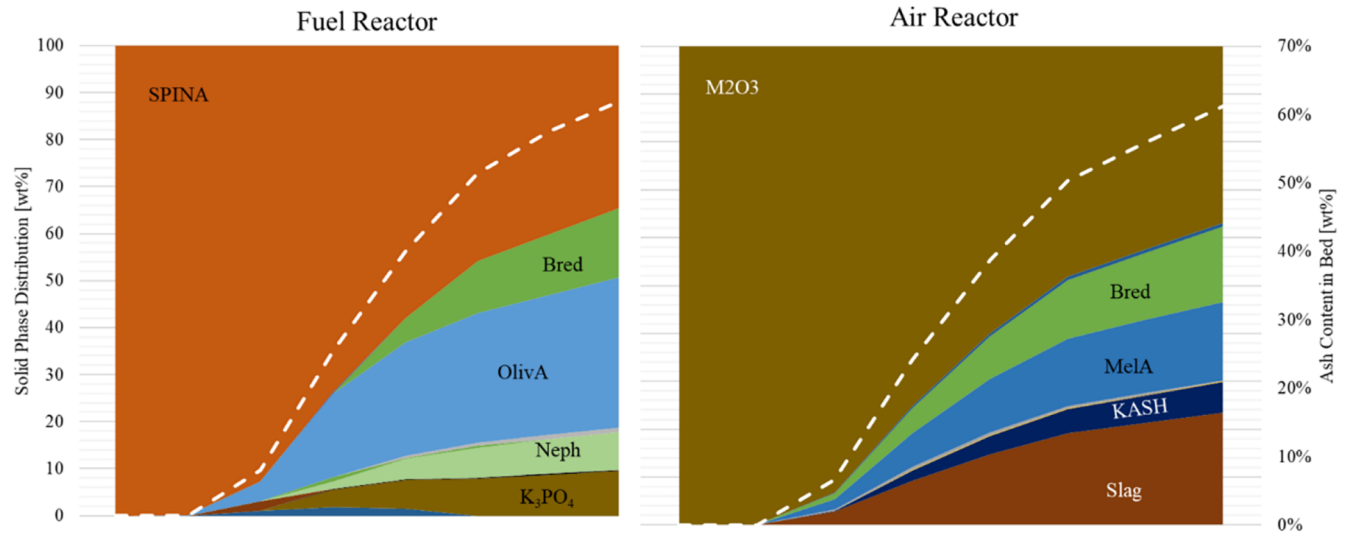

Figure 2. Solid-phase distribution in a fuel reactor at 950 °C (left) and air reactor at 1050 °C (right) for CLC of branches and treetops (BT) using iron oxide as an oxygen carrier. The ash content in the bed (dashed white line) is presented in the secondary y-axis.

the FR, the phases olivine, nepheline, bredigite (see Table S3), and K_3PO_4 increase. In the AR, the most stable phases are melilite, KASH [$(K, Na)AlSiO_4$], and slag, while the iron is maintained as Fe_2O_3. In the AR, the potassium phosphate becomes a slag due to higher temperatures and oxidizing conditions. For all cases, Fe_2SiO_4 is the major ash-induced phase and is of particular importance for this work as the main active oxygen carrier metal would be affected. This also indicates that a certain amount of Si would enter the AR where the elevated temperature could lead to melting since Fe_2SiO_4 is

oxidized to Fe_2O_3 and SiO_2. Previous laboratory-scale experiments[37] performed at 950 °C and in the same reducing environment using K_2CO_3, SiO_2, and Fe_2O_3 showed the formation of Fe_2SiO_4 after reduction but not after oxidation. Other researchers have also observed Fe_2SiO_4 when using iron oxide in CLC of coal and observed that Fe_2SiO_4 could be regenerated to Fe_2O_3 + SiO_2 in the AR,[55] consistent with results here as olivine is transformed to Fe_2O_3 and SiO_2 (which becomes a part of the slag).
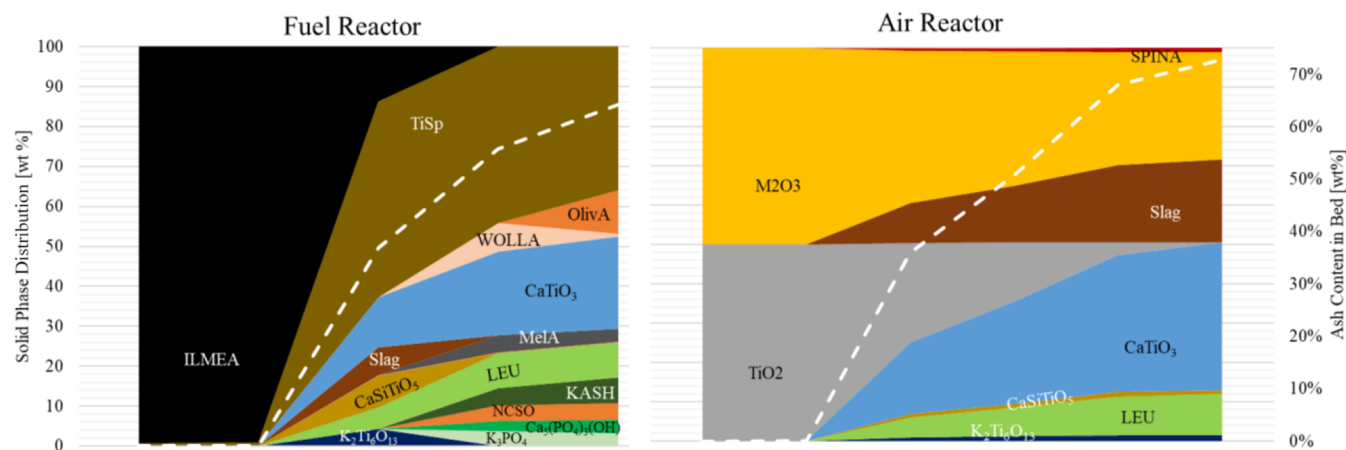
Figure 3. Solid-phase distribution in a fuel reactor at 950 °C (left) and air reactor at 1050 °C (right) for CLC of branches and treetops (BT) using ilmenite as an oxygen carrier. The ash content in the bed (dashed white line) is presented in the secondary y-axis.

3.2. Chemical Looping Combustion Using Ilmenite.

The reduced form of ilmenite is $FeTiO_3$ at prevailing conditions in the fuel reactor (see the phase diagram in Figure S4). From Figure S4, an intermediate phase, spinel and rutile $(Fe_3O_4 + TiO_2)$, is observed before reduction to $FeTiO_3$. Although a 1:1 fraction of Fe/Ti is relevant for ilmenite, the ash will elevate the Fe content in the bed. This causes titania spinel $((Fe, Ti)_3O_4)$ and spinel (Fe_3O_4) to become the most reduced phases. The solid-phase distribution in the FR and AR for BT is presented in Figure 3, and results for RWW and MSW are presented in Figures S5 and S6. Compared with the results with iron oxide, the presence of Ti makes a significant impact on the phase distribution. In an ilmenite bed, an increasing amount of ash results in $CaTiO_3$ (for BT), $K_2Ti_6O_{13}$, and $CaSiTiO_5$, which are present in both the FR and AR. The stability of these phases prevents the reduction back to $FeTiO_3$ but stabilizes K and Ca in the ilmenite structure. The formation of potassium and calcium titanates has previously been observed during OCAC operation with ilmenite (see Table 2). The titania spinel is oxidized to Fe_2O_3, TiO_2, and $CaTiO_3$ in the air reactor. The formation of the spinel is due to the high metal content in the ashes allowing $(Zn, Mg, Al)Fe_2O_4$ to form. With increasing ash content, the spinel becomes stable even in the AR, preventing complete oxidation to Fe_2O_3.

3.3. Fate of Ash Components.

The minor ash elements S, K, Na, Cl, Pb, Cu, and Zn are of particular importance with respect to boiler chemistry. The elemental distribution of these elements and their relationship will be discussed in the following sections. The total release to the gas phase for each element is presented in Table 3. BT contains the lowest amount of S, Cl, and ash and MSW the highest. Note that if the release is 100% for BT, the total weight released can still be lower compared with RWW or MSW. This is illustrated by the colors where green corresponds to the highest released weight and red the lowest released weight, and the clear cells represent the gas-phase release in between. It is evident from the table that CLC of MSW will have the most inorganic elements present in the gas phase of the FR. The table shows that CLC of RWW using $FeTiO_3$ as an OC will result in the least amount of K but the highest amount of Zn in the gas phase. Pb remains unaffected by the OC or fuel type. Specific solid and gas phases

Table 3. Weight Percent of Elements Released to the Gas Phase in the Fuel Reactor, at the Lowest Ash Concentration, for the Oxygen Carriers Ilmenite and Iron Oxide[a]

Release to the gas phase [wt% of the total amount]	BT		RWW		MSW	
Oxygen Carrier	Iron oxide	Ilmenite	Iron oxide	Ilmenite	Iron oxide	Ilmenite
S	99.98	99.97	62.33	96.7	86.61	83.67
Cl	100	100	100	100	100	100
K	13.1	0.89	11.7	6.8	46.29	4
Na	2.13	0.35	1.9	4.4	6	0.9
Zn	0.1	98.94	0.03	29.7	0.04	66.5
Cu	0.6	0.47	0.1	0	0.05	0.1
Pb	100	99.99	99.96	99.3	99.36	97.6

[a]The highest (green) and lowest (red) weights released are indicated.

for different ash concentrations are presented in Tables S7−S13 for iron oxide and Tables S14−S20 for ilmenite.

In the following sections, important elements will be discussed individually along with correlations with the literature.

Sulfur. Different reaction paths and the influence of the oxygen carrier on the sulfur phase formations are presented in Figure 4. For both ilmenite and iron oxide, a major part is released to the gas phase in the FR as H_2S while a small amount is transferred to the AR as FeS/ZnS or slag. In the AR, the sulfides are oxidized to Fe_2O_3/ZnO, leaving SO_2 to form K_2SO_4. The major metal compound in the FR is PbS (g) and the PbS concentration is the highest for MSW. There is a clear difference for the OCs where FeS and Cu_5FeS_4 form only for the case with iron oxide. This is especially clear for RWW (Table 3), and as a result, higher SO_2 concentrations are encountered in the AR. There is a clear difference between the K_2SO_4 concentration in the AR where the combination of iron oxide and BT causes the highest gas-phase release, whereas ilmenite does not due to the formation of potassium titanate $K_2Ti_6O_{13}$ or $KTi_8O_{16.5}$ (see the discussion regarding potassium below). Calcium and potassium sulfates can accumulate in ilmenite during OCAC, which has been shown by Vigoureux et al.[30] A detailed sulfur phase distribution can be found in the SI—Table S7 for iron oxide and Table S14 for ilmenite.

Chlorine. Chlorine is completely released to the gas phase in the FR for all OC−fuel combinations. It is known that the affinity of alkali metals toward chlorine is high, and
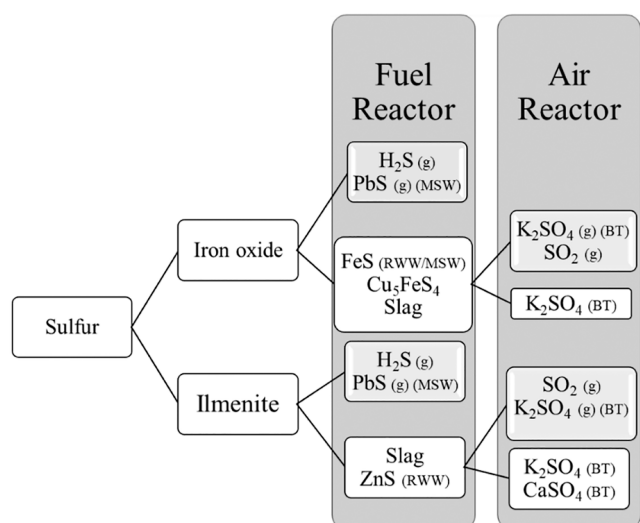
Figure 4. Summary of possible sulfur pathways in CLC and the influence of the bed material. Fuel-specific phases are denoted by fuel abbreviations in brackets.

accordingly, the major phase is KCl. The KCl concentration increases while the HCl concentration decreases according to MSW < RWW < BT for both OCs. There is a clear difference between the alkali metals; for example, the amount of NaCl is always lower than KCl (see Figure 5). There are also
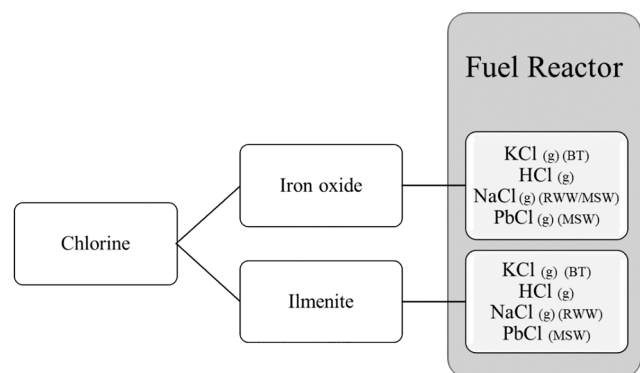

Figure 5. Summary of possible chlorine pathways in CLC and the influence of the bed material. Fuel-specific phases are denoted by fuel abbreviations in brackets.

differences between the fuels. For BT, with the lowest Cl content, the main component is KCl which increases with the ash content. For RWW, the distribution is equal between HCl, NaCl, and KCl. With increasing ash content, the amount of HCl dominates, and PbCl increases. For MSW, HCl is the major component. In this case, the amount of PbCl increases with increased ash levels. There are also differences between the OCs. Ilmenite causes higher HCl concentrations, especially for MSW, compared with iron oxide, which has higher (K, Na) Cl concentrations. The results here indicate that a significant fraction of the corrosive compounds will be concentrated in the FR outlet. The worst corrosion-related issues are expected in the FR for all fuels using iron oxide. The gas-phase release of alkali metals is shown to be lower when utilizing ilmenite as an OC. A detailed chlorine phase distribution can be found in the SI—Table S8 for iron oxide and Table S15 for ilmenite.

Potassium. The potassium phase distribution heavily depends on the composition of the ashes but also the oxygen carrier. Due to large fuel variations, the behavior differs in each case. For BT, a small amount is released as KOH and KCl, and the rest is associated with slag as K_2O or $K_3PO_4/K_2Ti_6O_{13}$ for iron oxide/ilmenite, respectively. There is also a difference between the OCs. The titanium content in ilmenite allows for potassium titanate to form, something which has been observed experimentally when ilmenite has been used in OCAC of biomass (see Table 2). The positive effects of ilmenite on potassium gas-phase release have also been discussed in the literature[25] and are also something that is predicted here (see Table 3 and Figure 6). In the AR, the
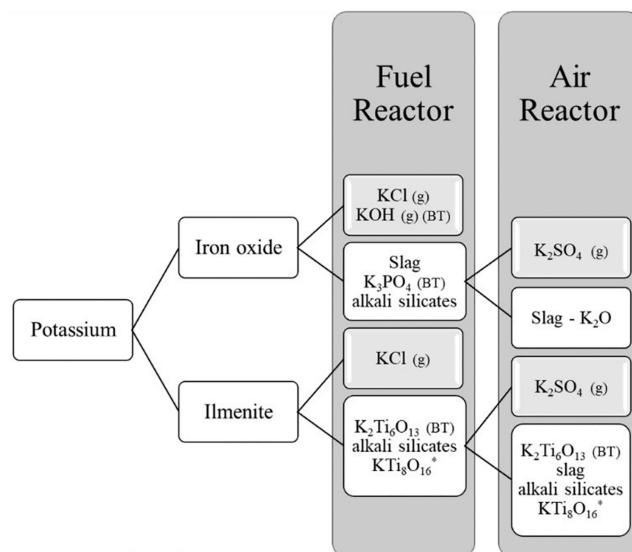

Figure 6. Summary of possible potassium pathways in CLC and the influence of the bed material. Alkali silicates include feldspar, nepheline, and leucite. Fuel-specific phases are denoted by fuel abbreviations in brackets. KTi_8O_{16}* is stable at reducing conditions and low K concentrations, which can be encountered inside ilmenite particles.

potassium titanate remains stable, and the small amount of potassium released to the gas phase is in the form of K_2SO_4. For both OCs, increasing the ash content results in silicates such as $KAlSiO_4$, $KAlSi_2O_6$, and $KAlSi_3O_8$. A detailed potassium phase distribution can be found in the SI—Table S9 for iron oxide and Table S16 for ilmenite.

Sodium. Sodium is concentrated in the slag phase for iron oxide, in both the FR and AR. An increase in temperature and oxygen availability increases the risk of melts which is seen in the AR where a major part of Na is found in the slag as Na_2O for both OCs (see Figure 7). However, in the presence of ilmenite, sodium silicates are more stable in the FR, since ilmenite does not take up the Si as iron oxide does, which forms Fe_2SiO_4. There are also differences between the fuels. For BT and RWW, sodium phosphates, $Na_2CaP_2O_7$, are stable. The release to the gas phase is lower than for potassium, and no release is observed in the AR. Increasing the ash content increases the phases nepheline and feldspar, which are in equilibrium with the slag. There are available studies on iron oxide and CLC of coal where the nepheline phase has been reported[56] (see Table 2). A detailed sodium phase distribution can be found in the SI—Table S10 for iron oxide and Table S17 for ilmenite. It is shown here that the behavior of the alkali
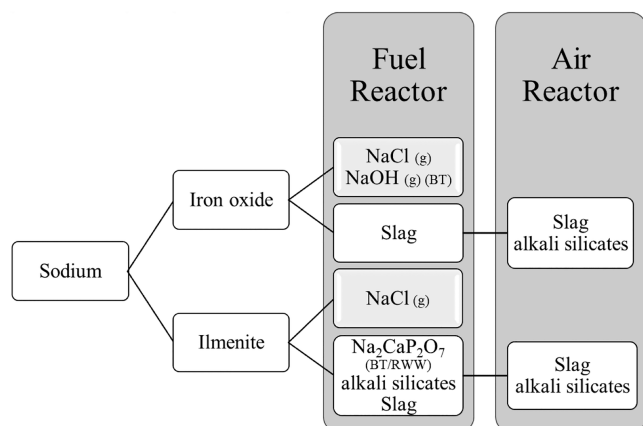
Figure 7. Summary of possible sodium pathways in CLC and the influence of the bed material. Alkali silicates include nepheline and feldspar. Fuel-specific phases are denoted by fuel abbreviations in brackets.

metals is not identical. For example, with ilmenite as an oxygen carrier, it is shown here that sodium is more inclined to form phosphates while potassium is more likely to be found in the form of titanates. Furthermore, the gas-phase release of potassium is always higher, especially in the AR.

Zinc. Zinc shows a clear difference in behavior between the two OCs, as seen in Figure 8. For iron oxide, almost no Zn is
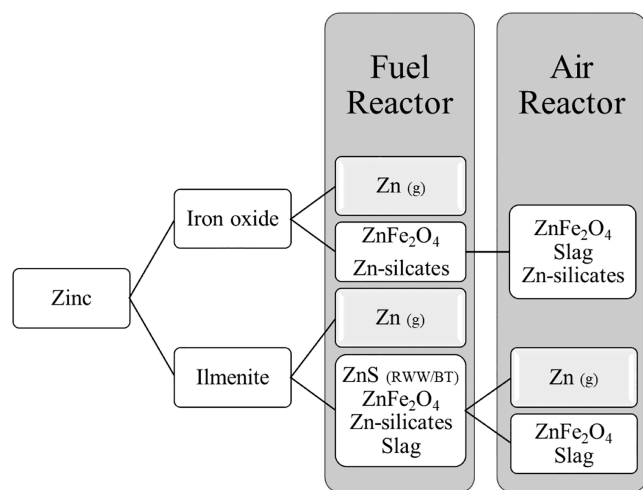

Figure 8. Summary of possible zinc pathways in CLC and the influence of the bed material. Fuel-specific phases are denoted by fuel abbreviations in brackets.

released to the gas phase [<0.1% is released as $Zn(g)$], and it is instead bound in the spinel structure as $ZnFe_2O_4$. For ilmenite, on the other hand, all Fe is bound in $FeTiO_3$ or $FeTi_2O_4$, which does not dissolve Zn. It instead forms solid ZnS and silicates such as willemite, olivine, and melilite. Increasing the ash concentrations shifts the stability toward slag and zinc silicates. These silicates are not as stable as the spinel, and thus, a major part is released into the gas. This is also observed in the AR where a majority of Zn is found in the spinel for both OCs. In the AR, oxidation of ilmenite forms hematite and rutile, meaning that Fe is free to interact, and the conditions between the OCs are more alike. Thus, the interaction between ilmenite and zinc is expected to dominate at oxidizing

conditions, which are most likely enhanced after several cycles when iron migrates to the particle surfaces. A detailed zinc phase distribution can be found in the SI—Table S11 for iron oxide and Table S18 for ilmenite.

Copper. A small amount of Cu is released to the gas phase for both OCs (Table 3) either in the form of CuCl or Cu and CuS (iron oxide). Several solid components form in the FR such as Cu, Cu_3As, and Cu_5FeS_4. The formation of Cu_5FeS_4 is specific for iron oxide, while Cu_2O in slag is more stable for ilmenite. Due to the high temperature in the AR, Cu is found as Cu_2O in the slag in all cases, and only a small amount is released into the gas (see Figure 9). In previous studies, copper
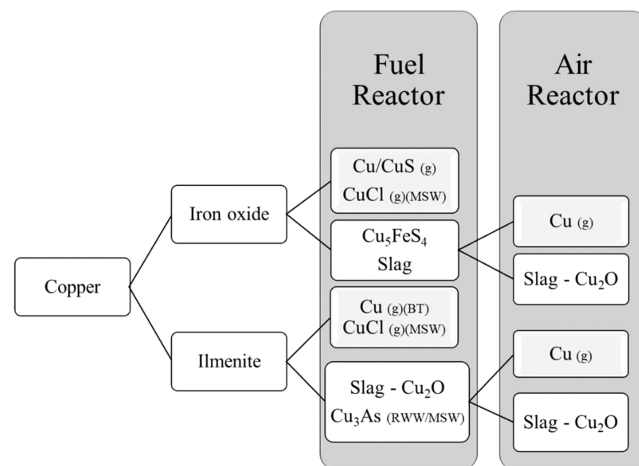

Figure 9. Summary of possible copper pathways in CLC and the influence of the bed material. Fuel-specific phases are denoted by fuel abbreviations in brackets.

ferrites have been reported for ilmenite used in OCAC of waste. However, with increasing reduction potential, copper ferrites are less stable. A detailed copper phase distribution can be found in the SI—Table S12 for iron oxide and Table S19 for ilmenite.

Lead. There are no significant differences between the OCs (see Figure 10). In all cases, a major amount of Pb (always over 97%) is released into the gas phase. The main gaseous component is PbS followed by Pb and PbCl. The small amount of slag (PbO) transferred to the AR will be released as $PbO(g)$. With increasing ash concentrations, more Pb will be associated
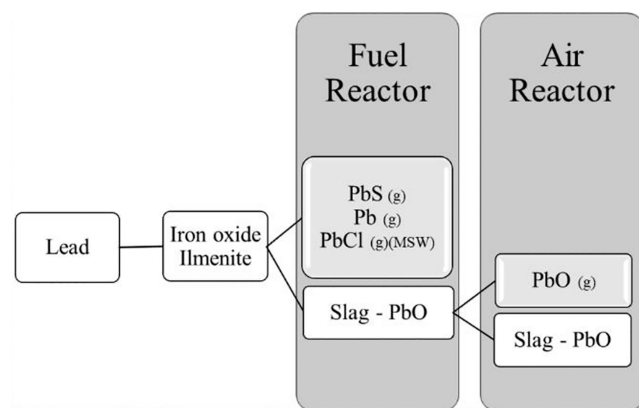

Figure 10. Summary of possible lead pathways in CLC. Fuel-specific phases are denoted by fuel abbreviations in brackets.

with solid phases such as melilite ($Pb_2FeSi_2O_7$), slag, and Pb(s). The highest amount of Pb in the gas phase is found in the case of MSW. A detailed lead phase distribution can be found in the SI—Table S13 for iron oxide and Table S20 for ilmenite.

3.4. Influence of Calculated Thermodynamic Data.

The enthalpy, entropy, and temperature-dependent heat capacities for the compounds KTi_8O_{16}, $KTi_8O_{16.5}$, $K_{0.85}Fe_{0.85}Ti_{0.15}O_2$, and $K_{0.4}Fe_{0.4}Ti_{0.6}O_2$ were added to the user-defined database in FactSage 8.1. The influence of the calculated data is presented in ternary phase diagrams for $Fe_2O_3-TiO_2-K_2O$ in Figures S7 and S8. As seen from the results in Section 3.3, none of the four compounds were found to be stable under prevailing conditions. Although these phases have been found in experimental works,[25,27,37] incorporation of the thermodynamic data did not show any stability. This is likely due to phases already incorporated in the common databases having lower Gibbs free energy under these conditions, or impurities combining with active elements and having higher stability. The two compounds $K_{0.85}Fe_{0.85}Ti_{0.15}O_2$ and $K_{0.4}Fe_{0.4}Ti_{0.6}O_2$ have been observed after batch experiments at 900 °C where a high amount of potassium carbonate was mixed with ilmenite.[37] Studying the ternary phase diagram $Fe_2O_3-TiO_2-K_2O$ at lower temperatures showed that $K_xFe_xTi_{1-x}O_2$ becomes stable at high K concentrations. However, the slag phase is stable under the same conditions, and it is therefore most likely that it prohibits $K_xFe_xTi_{1-x}O_2$. The two compounds KTi_8O_{16} and $KTi_8O_{16.5}$ have been observed after OCAC of wood chips.[25,27] Wood chips contain a small amount of ash and thus low K concentrations. Likely, the concentration of potassium in combination with effects related to local changes in the boiler provide conditions that are favorable for the formation of these compounds. The hypothesis is supported by the ternary phase diagram presented in Figure S8 where KTi_8O_{16} is found to be stable at low potassium concentrations and high titanium concentrations: conditions which can be encountered inside ilmenite particles, for example. The formation of KTi_8O_{16} will have implications for the behavior of potassium (see Figure 6), something which can have practical implications, not only for CLC but also for OCAC systems. When KTi_8O_{16} forms, it will retain potassium in the OC which will hinder the gas-phase release of potassium.

4. DISCUSSION

Iron-based oxygen carriers are particularly important oxygen carriers for CLC, primarily due to their high availability, low cost, and reasonable reactivity. Ilmenite can be considered a benchmark oxygen carrier, accelerated by its recent commercial use as an oxygen carrier in commercial OCAC units. Still, the knowledge of interaction pathways of reactive ash components from biomass is not complete. The authors have previously used thermodynamic tools in combination with detailed characterization to improve understanding, among other things, using improved and combined databases of thermodynamic data.[33] In this paper, a comprehensive overview of experimentally determined phases was conducted and compared to phases available in newly updated databases. To improve understanding further, a new method has been used to obtain the thermodynamic properties of compounds where no thermodynamic data have been reported. Here, first-principles calculations were made to establish heat of formation and heat capacity data as a function of temperature.

By doing so, the knowledge of iron-based oxygen carriers and their interaction with ash components has improved.

Thermodynamic calculations are useful and easy to use, but several limitations exist. For example, all elements are assumed to be perfectly mixed, and kinetic and transportation phenomena are neglected.[57] Therefore, global calculations with big relative variations between the elements considered may not fully reflect a real situation. The calculations do not consider the form of the participating elements that enter the FR, the time required for combustion, or the kinetics and transport phenomena. However, due to the good gas–solid contact, mixing, and relatively long residence times of solid particles in fluidized beds, the conditions could come close to equilibrium.[34] For the calculations with ilmenite, an equal amount of Fe and Ti is assumed to be available to interact with the ash. However, this may not be the case, as it is known from previous studies that Fe in ilmenite will migrate toward the surface of the particle, and a titanium-rich core will be created after a certain number of redox reactions. This will prevent Ti from directly interacting with the ash components, and elements would need to diffuse through the ash layer to do so. This is reflected in Figure 3, where titania-spinel, with a high content of Fe_3O_4, is formed with increasing ash concentration. In the AR, this phase is oxidized to Fe_2O_3 while the remaining Ti is found as $CaSiTiO_5$ or $CaTiO_3$ (for BT). When Ti is prevented from interacting with the ash, the resulting phases will be closer to the results with iron oxide.

The phases observed here can be divided into two different types of interaction between biomass/waste ash and iron-based OCs. Chemical interactions, for example, are distinguished by the interaction between the ash element and the OC: here, involving the formation of ferrites and titanates. Ash elements prone to form ferrites are, for example, Zn and Cu, while Ca and K form titanates. Physical interactions are characterized by, for example, sticky coatings on particles that do not chemically interact with the OC but rather stick to their surface. This is especially true for the predicted slag phase, which not only sticks to the OCs but is also a contributing factor for agglomeration. The silicates leucite, nepheline, and feldspar are in close equilibrium with the slag. While potassium titanates are the major OC-induced phase, potassium is also likely to be found in the slag or silicates along with sodium. Since biomass fuels generally contain higher concentrations of potassium, less focus has been on sodium and its interaction with OCs. However, when utilizing waste fuels, sodium concentrations can exceed those of potassium. It is shown here that while potassium is likely to form titanates in the case of ilmenite, sodium is more inclined to form phosphates. Furthermore, the gas-phase release of potassium is always higher compared to sodium. It is identified in this work that studies on the interaction between OCs and sodium are scarce and need further research.

4.1. Implications on Chemical Looping Combustion.

Alkali compounds are well-known precursors for producing low-melting compounds, which could be problematic in thermal conversion systems. Hence, the fate of alkali is of special importance to study. Comparing the total amount of alkali released for the two OCs, less K is released in the case of ilmenite. Previous studies have observed potassium titanates during OCAC operation with ilmenite (see Table 2). These compounds retain potassium in the bed, which has a positive effect on corrosion and fouling. The behavior of potassium varies largely between the oxygen carriers, which is due to the

complex relationship between the oxygen carrier, silicates, slag, and gaseous alkali components (chlorides, sulfates, hydroxides, etc.). For CLC of RWW using iron oxide, Si from the ash will combine with the bed material forming olivine (Fe_2SiO_4) leaving the alkali metals to equilibrate between the slag and the gas phase. For $FeTiO_3$, Si is free to form stable alkali silicates such as feldspar ($KAlSi_3O_8$), nepheline ($NaAlSiO_4$), and leucite ($K_2Al_2Si_4O_{12}$). When KTi_8O_{16} forms, it will retain potassium in the OC; otherwise, the formation of silicates is the main reason that less alkali is released to the gas phase. These silicates are preferable in the full-scale application as they will not cause agglomerations or operational issues in the boiler. However, research around the stability of these compounds in the presence of ilmenite needs to be evaluated experimentally. For both oxygen carriers, the most corrosive compounds are expected to leave with the gas in the FR, leaving the AR free from corrosive chlorides. In the AR, temperatures are inevitably higher, and the risk of melt formation and thus agglomeration increases, especially with higher ash concentrations. One solution to this could be to lower the temperature in the AR, but an elevated temperature is needed here as most of the heat is extracted in this reactor. Another possibility is to effectively separate the OC from the ash. In this study, a range of different ash concentrations has been investigated, although in a real system, it is expected that the ash is separated from the OC before returning the reduced OC to the AR. One way to separate the OCs from the ash is by using a magnetic separator. With this method, ash components such as alkali silicates could be separated from the OC. By lowering the ash concentrations, melts can be avoided, and the most relevant results of this study would be located on the far left of Figure 2.

5. CONCLUSIONS

The fate of several ash components in CLC of biomass and waste utilizing two iron-based oxygen carriers, iron oxide and ilmenite, has been studied using multicomponent multiphase equilibrium calculations. The incorporation of first-principles thermodynamic data of identified crystalline phases in the overall thermodynamic calculations has contributed to the most comprehensive and updated thermodynamic study of these important systems to date. The fate of ash elements was affected by the type of oxygen carrier. For example, compared with iron oxide, a large share of Zn is released to the gas phase in the case of ilmenite while a larger portion of potassium is retained in the solid phases. The titanium content influences the distribution directly, by forming calcium and alkali titanates, and indirectly, by forming iron titanates and not iron silicates, freeing silicon to interact with the alkali metals. For both oxygen carriers, the most corrosive compounds are expected to leave with the gas in the FR. Issues related to corrosion and fouling are expected to be concentrated in the FR, which is beneficial as most of the heat is extracted from the AR. This paper also illustrates the importance of ash separation due to the high agglomeration tendencies in the AR. Factors investigated in this study are useful in determining and optimizing the operating conditions for biowaste-fueled CLC to prevent defluidization, agglomeration, and corrosion.

ASSOCIATED CONTENT

ⓢ Supporting Information

The Supporting Information is available free of charge at https://pubs.acs.org/doi/10.1021/acs.energyfuels.2c01578.

Thermal properties of KTi_8O_{16}, $KTi_8O_{16.5}$, $K_{0.85}Fe_{0.85}Ti_{0.15}O_2$, $K_{0.4}Fe_{0.4}Ti_{0.6}O_2$, and $FeTiO_3$; gas-phase compositions reported in the literature; solid solutions and their abbreviations; solid phases for BT, RWW, and MSW; elemental phase distributions; phase diagrams; solid-phase distributions; and ternary phase diagrams (PDF)

AUTHOR INFORMATION

Corresponding Author

Ivana Staničić − *Department of Space, Earth and Environment, Division of Energy Technology, Chalmers University of Technology, SE-412 96 Gothenburg, Sweden;* ⓞ orcid.org/0000-0002-6927-4822; Email: stanicic@chalmers.se

Authors

Joakim Brorsson − *Department of Physics, Division of Chemical Physics, Chalmers University of Technology, SE-412 96 Gothenburg, Sweden*

Anders Hellman − *Department of Physics, Division of Chemical Physics, Chalmers University of Technology, SE-412 96 Gothenburg, Sweden;* ⓞ orcid.org/0000-0002-1821-159X

Tobias Mattisson − *Department of Space, Earth and Environment, Division of Energy Technology, Chalmers University of Technology, SE-412 96 Gothenburg, Sweden;* ⓞ orcid.org/0000-0003-3942-7434

Rainer Backman − *Department of Applied Physics and Electronics, Thermochemical Energy Conversion Laboratory, Umeå University, SE-901 87 Umeå, Sweden*

Complete contact information is available at:
https://pubs.acs.org/10.1021/acs.energyfuels.2c01578

Author Contributions

The manuscript was written with the contributions of all authors. All authors have approved the final version of the manuscript.

Notes

The authors declare no competing financial interest.

ABBREVIATIONS

CLC = chemical looping combustion
OCAC = oxygen carrier aided combustion
OC = oxygen carrier
FR = fuel reactor
AR = air reactor
CCS = carbon capture and storage
CLOU = chemical looping with oxygen uncoupling
WtE = waste-to-energy

REFERENCES

(1) Rydén, M.; Lyngfelt, A.; Langørgen, Ø.; Larring, Y.; Brink, A.; Teire, S.; Havågf, H.; Karmhageng, P. Negative CO2 Emissions with Chemical-Looping Combustion of Biomass − a Nordic Energy Research Flagship Project. *Energy Procedia* **2017**, *114*, 6074−6082.

(2) Kemper, J. Biomass and carbon dioxide capture and storage: A review. *International Journal of Greenhouse Gas Control* **2015**, *40*, 401−430.

(3) Abanades, J. C.; Arias, B.; Lyngfelt, A.; Mattisson, T.; Wiley, D. E.; Li, H.; Ho, M. T.; Mangano, E.; Brandani, S. Emerging CO2 capture systems. *International Journal of Greenhouse Gas Control* **2015**, *40*, 126−166.

(4) *On the promotion of the use of energy from renewable sources (recast)*; COM (2016) 767; Directive of the European Parliament and of the Council (European Commission), 2016; Climate Change 2014: Synthesis Report; Contribution of Working Groups I, II and III to the Fifth Assessment Report of the Intergovernmental Panel on Climate Change; IPCC, 2016.

(5) Abanades, J.; Arias, B.; Lyngfelt, A.; Mattisson, T.; Wiley, D.; Li, H.; Ho, M.; Mangano, E.; Brandani, S. Emerging CO2 capture systems. *International Journal of Greenhouse Gas Control* **2015**, *40*, 126−166.

(6) Khan, A. A.; de Jong, W.; Jansens, P. J.; Spliethoff, H. Biomass combustion in fluidized bed boilers: Potential problems and remedies. *Fuel Process. Technol.* **2009**, *90* (1), 21−50.

(7) Spiegel, M. Corrosion in Molten Salts. In *Shreir's Corrosion*; Cottis, B., Graham, M., Lindsay, R., Lyon, S., Richardson, T., Scantlebury, D., Stott, H., Eds.; Elsevier, 2010; Chapter 1.14, pp 316−330.

(8) Kinnunen, H.; Hedman, M.; Lindberg, D.; Enestam, S.; Yrjas, P. Corrosion in Recycled Wood Combustion—Reasons, Consequences, and Solutions. *Energy Fuels* **2019**, *33* (7), 5859−5866.

(9) Niu, Y.; Tan, H.; Hui, S. Ash-related issues during biomass combustion: Alkali-induced slagging, silicate melt-induced slagging (ash fusion), agglomeration, corrosion, ash utilization, and related countermeasures. *Prog. Energy Combust. Sci.* **2016**, *52*, 1−61.

(10) Gatternig, B.; Karl, J. Investigations on the mechanisms of ash-induced agglomeration in fluidized-bed combustion of biomass. *Energy Fuels* **2015**, *29* (2), 931−941.

(11) Dong, C.; Jiang, J.; Yang, Y.; Zhang, J.; Shan, L. In *Research on the reactivity of oxygen carrier Fe2O3 for chemical looping combustion (CLC)*, Asia-Pacific Power and Energy Engineering Conference; APPEEC, 2010. DOI: 10.1109/APPEEC.2010.5448948.

(12) Jerndal, E.; Mattisson, T.; Lyngfelt, A. Thermal Analysis of Chemical-Looping Combustion. *Chem. Eng. Res. Des.* **2006**, *84* (9), 795−806.

(13) Abad, A.; Adánez, J.; García-Labiano, F.; de Diego, L. F.; Gayán, P.; Celaya, J. Mapping of the range of operational conditions for Cu-, Fe-, and Ni-based oxygen carriers in chemical-looping combustion. *Chem. Eng. Sci.* **2007**, *62* (1−2), 533−549.

(14) Mendiara, T.; Abad, A.; de Diego, L. F.; García-Labiano, F.; Gayán, P.; Adánez, J. Biomass combustion in a CLC system using an iron ore as an oxygen carrier. *International Journal of Greenhouse Gas Control* **2013**, *19*, 322−330.

(15) Linderholm, C.; Schmitz, M. Chemical-looping combustion of solid fuels in a 100 kW dual circulating fluidized bed system using iron ore as oxygen carrier. *Journal of Environmental Chemical Engineering* **2016**, *4* (1), 1029−1039.

(16) Bao, J.; Li, Z.; Cai, N. Interaction between iron-based oxygen carrier and four coal ashes during chemical looping combustion. *Applied Energy* **2014**, *115*, 549−558.

(17) Gu, H.; Shen, L.; Zhong, Z.; Zhou, Y.; Liu, W.; Niu, X.; Ge, H.; Jiang, S.; Wang, L. Interaction between biomass ash and iron ore oxygen carrier during chemical looping combustion. *Chemical Engineering Journal* **2015**, *277*, 70−78.

(18) Hanning, M.; Gyllén, A.; Lind, F.; Rydén, M. Biomass ash interactions with a manganese ore used as oxygen-carrying bed material in a 12 MW th CFB boiler. *Biomass and Bioenergy* **2018**, *119*, 179−190.

(19) Knutsson, P.; Linderholm, C. Characterization of ilmenite used as oxygen carrier in a 100 kW chemical-looping combustor for solid fuels. *Applied Energy* **2015**, *157*, 368−373.

(20) Cuadrat, A.; Abad, A.; García-Labiano, F.; Gayán, P.; de Diego, L. F.; Adánez, J. The use of ilmenite as oxygen-carrier in a 500Wth

Chemical-Looping Coal Combustion unit. *International Journal of Greenhouse Gas Control* **2011**, *5* (6), 1630−1642.

(21) Moldenhauer, P.; Rydén, M.; Mattisson, T.; Younes, M.; Lyngfelt, A. The use of ilmenite as oxygen carrier with kerosene in a 300 W CLC laboratory reactor with continuous circulation. *Applied Energy* **2014**, *113* (0), 1846−1854.

(22) Liu, F.; Zhang, Y.; Chen, L.; Qian, D.; Neathery, J. K.; Kozo, S.; Liu, K. Investigation of a Canadian ilmenite as an oxygen carrier for chemical looping combustion. *Energy Fuels* **2013**, *27* (10), 5987−5995.

(23) Thunman, H.; Lind, F.; Breitholtz, C.; Berguerand, N.; Seemann, M. Using an oxygen-carrier as bed material for combustion of biomass in a 12-MWth circulating fluidized-bed boiler. *Fuel* **2013**, *113*, 300−309.

(24) Lind, F.; Corcoran, A.; Andersson, B.; Thunman, H. 12,000 h of Operation with Oxygen-Carriers in Industrially Relevant Scale (75,000 kWth). *VGB PowerTech* **2017**, (7), 82−87.

(25) Corcoran, A.; Marinkovic, J.; Lind, F.; Thunman, H.; Knutsson, P.; Seemann, M. Ash properties of ilmenite used as bed material for combustion of biomass in a circulating fluidized bed boiler. *Energy Fuels* **2014**, *28* (12), 7672−7679.

(26) Gyllén, A.; Knutsson, P.; Lind, F.; Thunman, H. Magnetic separation of ilmenite used as oxygen carrier during combustion of biomass and the effect of ash layer buildup on its activity and mechanical strength. *Fuel* **2020**, *269*, 117470.

(27) Corcoran, A.; Knutsson, P.; Lind, F.; Thunman, H. Mechanism for migration and layer growth of biomass ash on ilmenite used for oxygen carrier aided combustion. *Energy Fuels* **2018**, *32* (8), 8845−8856.

(28) Samprón, I.; de Diego, L. F.; García-Labiano, F.; Izquierdo, M. T. Effect of the Fe content on the behavior of synthetic oxygen carriers in a 1.5 kW biomass chemical looping gasification unit. *Fuel* **2022**, *309*, 122193.

(29) Hildor, F.; Zevenhoven, M.; Brink, A.; Hupa, L.; Leion, H. Understanding the Interaction of Potassium Salts with an Ilmenite Oxygen Carrier Under Dry and Wet Conditions. *ACS Omega* **2020**, *5* (36), 22966−22977.

(30) Vigoureux, M.; Knutsson, P.; Lind, F. Sulfur Uptake during Oxygen-Carrier-Aided Combustion with Ilmenite. *Energy Fuels* **2020**, *34* (6), 7735−7742.

(31) Staničić, I.; Mattisson, T.; Backman, R.; Cao, Y.; Rydén, M. Oxygen carrier aided combustion (OCAC) of two waste fuels - Experimental and theoretical study of the interaction between ilmenite and zinc, copper and lead. *Biomass and Bioenergy* **2021**, *148*, 106060.

(32) Staničić, I.; Cañete Vela, I.; Backman, R.; Maric, J.; Cao, Y.; Mattisson, T. Fate of lead, copper, zinc and antimony during chemical looping gasification of automotive shredder residue. *Fuel* **2021**, *302*, 121147.

(33) Staničić, I.; Backman, R.; Cao, Y.; Rydén, M.; Aronsson, J.; Mattisson, T. Fate of trace elements in Oxygen Carrier Aided Combustion (OCAC) of municipal solid waste. *Fuel* **2021**, *311*, 122551.

(34) Moradian, F.; Tchoffor, P. A.; Davidsson, K. O.; Pettersson, A.; Backman, R. Thermodynamic equilibrium prediction of bed agglomeration tendency in dual fluidized-bed gasification of forest residues. *Fuel Process. Technol.* **2016**, *154*, 82−90.

(35) Lindberg, D.; Backman, R.; Chartrand, P.; Hupa, M. Towards a comprehensive thermodynamic database for ash-forming elements in biomass and waste combustion — Current situation and future developments. *Fuel Process. Technol.* **2013**, *105*, 129−141.

(36) Staničić, I.; Andersson, V.; Hanning, M.; Mattisson, T.; Backman, R.; Leion, H. Combined manganese oxides as oxygen carriers for biomass combustion — Ash interactions. *Chem. Eng. Res. Des.* **2019**, *149*, 104−120.

(37) Staničić, I.; Hanning, M.; Deniz, R.; Mattisson, T.; Backman, R.; Leion, H. Interaction of oxygen carriers with common biomass ash components. *Fuel Process. Technol.* **2020**, *200*, 106313.

(38) Kennedy, J. R.; Khadilkar, A. B.; Bhattacharya, S.; Pisupati, S. V. Modeling the Impact of Operating Variables on Ash Agglomeration in Chemical Looping Combustion of Solid Fuels. *Ind. Eng. Chem. Res.* **2021**, *60* (49), 17970−17979.

(39) Khadilkar, A. B.; Rozelle, P. L.; Pisupati, S. V. A study on initiation of ash agglomeration in fluidized bed gasification systems. *Fuel* **2015**, *152*, 48−57.

(40) Linstrom, P. J.; Mallard, W. G. The NIST Chemistry WebBook: A Chemical Data Resource on the Internet. *Journal of Chemical & Engineering Data* **2001**, *46* (5), 1059−1063.

(41) Krzystowczyk, E.; Wang, X.; Dou, J.; Haribal, V.; Li, F. Substituted SrFeO3 as robust oxygen sorbents for thermochemical air separation: correlating redox performance with compositional and structural properties. *Phys. Chem. Chem. Phys.* **2020**, *22* (16), 8924−8932.

(42) Wang, X.; Gao, Y.; Krzystowczyk, E.; Iftikhar, S.; Dou, J.; Cai, R.; Wang, H.; Ruan, C.; Ye, S.; Li, F. High-throughput oxygen chemical potential engineering of perovskite oxides for chemical looping applications. *Energy Environ. Sci.* **2022**, *15* (4), 1512−1528.

(43) Li, F.; Sun, Z.; Luo, S.; Fan, L.-S. Ionic diffusion in the oxidation of iron—effect of support and its implications to chemical looping applications. *Energy Environ. Sci.* **2011**, *4* (3), 876−880.

(44) Benisek, A.; Dachs, E. The accuracy of standard enthalpies and entropies for phases of petrological interest derived from density-functional calculations. *Contributions to Mineralogy and Petrology* **2018**, *173* (11), 90.

(45) Li, X.; Lyngfelt, A.; Mattisson, T. An experimental study of a volatiles distributor for solid fuels chemical-looping combustion process. *Fuel Process. Technol.* **2021**, *220*, 106898.

(46) Nemati, N.; Rydén, M. Chemical-looping combustion in packed-fluidized beds: Experiments with random packings in bubbling bed. *Fuel Process. Technol.* **2021**, *222*, 106978.

(47) Lyngfelt, A.; Leckner, B. A 1000 MWth boiler for chemical-looping combustion of solid fuels − Discussion of design and costs. *Applied Energy* **2015**, *157*, 475−487.

(48) Niu, X.; Shen, L.; Gu, H.; Jiang, S.; Xiao, J. Characteristics of hematite and fly ash during chemical looping combustion of sewage sludge. *Chemical Engineering Journal* **2015**, *268*, 236−244.

(49) Störner, F.; Hildor, F.; Leion, H.; Zevenhoven, M.; Hupa, L.; Rydén, M. Potassium Ash Interactions with Oxygen Carriers Steel Converter Slag and Iron Mill Scale in Chemical-Looping Combustion of Biomass—Experimental Evaluation Using Model Compounds. *Energy Fuels* **2020**, *34* (2), 2304−2314.

(50) Adánez, J.; Cuadrat, A.; Abad, A.; Gayán, P.; Diego, L. F. D.; García-Labiano, F. Ilmenite activation during consecutive redox cycles in chemical-looping combustion. *Energy Fuels* **2010**, *24* (2), 1402−1413.

(51) Wang, H.; Liu, G.; Veksha, A.; Dou, X.; Giannis, A.; Lim, T. T.; Lisak, G. Iron ore modified with alkaline earth metals for the chemical looping combustion of municipal solid waste derived syngas. *Journal of Cleaner Production* **2021**, *282*, 124467.

(52) Chiwandika, E. K.; Jung, S. M. Perovskite Formation in Hematite−Ilmenite Ores Sintered in Argon. *Journal of Sustainable Metallurgy* **2022**, *8* (1), 310−320.

(53) Garcia, E.; Liu, H. Ilmenite as alternative bed material for the combustion of coal and biomass blends in a fluidised bed combustor to improve combustion performance and reduce agglomeration tendency. *Energy* **2022**, *239*, 121913.

(54) Hedayati, A.; Soleimanisalim, A. H.; Mattisson, T.; Lyngfelt, A. Thermochemical conversion of biomass volatiles via chemical looping: Comparison of ilmenite and steel converter waste materials as oxygen carriers. *Fuel* **2022**, *313*, 122638.

(55) Song, T.; Wu, J.; Zhang, H.; Shen, L. Characterization of an Australia hematite oxygen carrier in chemical looping combustion with coal. *International Journal of Greenhouse Gas Control* **2012**, *11*, 326−336.

(56) Yan, J.; Ge, H.; Jiang, S.; Gu, H.; Song, T.; Guo, Q.; Shen, L. Effect of Sodium Removal on Chemical Looping Combustion of High-Sodium Coal with Hematite as an Oxygen Carrier. *Energy Fuels* **2019**, *33* (3), 2153−2165.

(57) Vassilev, S. V.; Baxter, D.; Vassileva, C. G. An overview of the behaviour of biomass during combustion: Part I. Phase-mineral transformations of organic and inorganic matter. *Fuel* **2013**, *112*, 391−449.

🕮 Recommended by ACS

Potassium Ash Interactions with Oxygen Carriers Steel Converter Slag and Iron Mill Scale in Chemical-Looping Combustion of Biomass—Experimental Evaluation U...

Felicia Störner, Magnus Rydén, *et al.*

JANUARY 09, 2020
ENERGY & FUELS   READ 🗗

Interaction of Iron Oxygen Carriers and Alkaline Salts Present in Biomass-Derived Ash

Duygu Yilmaz and Henrik Leion

AUGUST 04, 2020
ENERGY & FUELS   READ 🗗

Sulfur Transformation Behavior of Inorganic Sulfur-Containing Compounds in Chemical Looping Combustion

Chao Wang, Haiyan Zhang, *et al.*

FEBRUARY 07, 2020
ENERGY & FUELS   READ 🗗

Experimental and Thermodynamic Study on the Interaction of Copper Oxygen Carriers and Alkaline-Containing Salts Commonly Present in Ashes

Duygu Yilmaz, Henrik Leion, *et al.*

MARCH 09, 2020
ENERGY & FUELS   READ 🗗

Get More Suggestions >